International Journal of Biological Macromolecules 242 (2023) 125049

Contents lists available at ScienceDirect

International Journal of Biological Macromolecules

journal homepage: www.elsevier.com/locate/ijbiomac

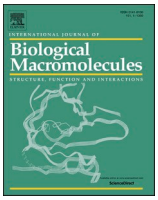

Designing antimicrobial biomembranes via clustering amino-modified cellulose nanocrystals on silk fibroin β-sheets

Estela O. Carvalho [a,b,c], Mikel Rincón-Iglesias [d], Ricardo Brito-Pereira [a,b,c,e,f], Erlantz Lizundia [d,g], Margarida M. Fernandes [a,b,c,e,f,*], Senentxu Lanceros-Mendez [d,h]

[a] Physics Centre of Minho and Porto Universities (CF-UM-UP), Universidade do Minho, 4710-057, Portugal
[b] LaPMET - Laboratory of Physics for Materials and Emergent Technologies, Universidade do Minho, 4710-057, Portugal
[c] IB-S – Institute for Research and Innovation on Bio-Sustainability, University of Minho, Braga 4710-057, Portugal
[d] BCMaterials, Basque Center Centre for Materials, Applications and Nanostructures, UPV/EHU Science Park, Leioa 48940, Spain
[e] Centre for MicroElectroMechanics Systems (CMEMS), University of Minho, Braga 4710-057, Portugal
[f] LABBELS-Associate Laboratory, Braga, Guimarães, Portugal
[g] Life Cycle Thinking Group, Department of Graphic Design and Engineering Projects, University of the Basque Country (UPV/EHU), Plaza Ingeniero Torres Quevedo 1, 48013 Bilbao, Biscay, Spain
[h] Ikerbasque, Basque Foundation for Science, 48009 Bilbao, Spain

ARTICLE INFO

Keywords:
Silk fibroin
Amine-functionalized cellulose
Blends
Antibacterial
Non-cytotoxic
Sustainable material

ABSTRACT

The continuous rising of infections caused by multidrug-resistant pathogens is becoming a global healthcare concern. Developing new bio-based materials with unique chemical and structural features that allow efficient interaction with bacteria is thus important for fighting this phenomenon. To address this issue, we report an antimicrobial biomaterial that results from clustering local facial amphiphilicity from amino-modified cellulose on silk fibroin β-sheets, by simply blending the two components through casting technology. A simple but effective method for creating a membrane that is antibacterial and non-cytotoxic. Amino-modified cellulose nanocrystals (CNC-NH_2) were mixed with proteinaceous silk fibroin (SF) which resulted in a material with improved crystallinity, higher β-sheet content, and exposed amino-groups at its surface features, proven by Fourier transform infrared (FTIR) spectroscopy and X-ray photoelectron spectroscopy (XPS), that does not occur when the components are individually assembled. The resulting material possesses important antibacterial activity inducing >3 CFU $\log_{10}$ reduction of *Escherichia coli* and *Staphylococcus epidermidis*, while the pristine membranes show no antibacterial effect. The chemical interactions occurring between SF and CNC-NH_2 during casting, exposing the amino moieties at the surface of the material, are proposed as the main reason for this antimicrobial activity. Importantly, the membranes are non-cytotoxic, showing their potential to be used as a new bioinspired material with intrinsic antibacterial activity for biomedical applications. Those may include coatings for medical devices for the control of healthcare-associated infections, with no need for including external antimicrobial agents in the material.

1. Introduction

Bacteria are essential for ecosystem preservation. However, the tiny number of bacteria capable of causing infections and diseases encompasses serious public health concerns [1]. Infections caused by drug-resistant bacteria are behind the increasing hospital mortality and morbidity, also inflicting a huge economic burden in clinical settings [2,3]. This phenomenon mostly results from the overuse and misuse of antibiotics which are losing their efficacy against an expanding range of pathogens [4].

Thus, strong efforts are being performed to tackle bacteria resistance by synthesizing new compounds which analogous to current antibiotics, but with slightly different structural and functional features. Nevertheless, this cannot be considered a long-term solution as the appearance of new resistant strains is predictable, requiring the continuous expenditure of time and resources [5,6]. A viable long-term alternative is the development of novel therapeutic techniques and materials capable of controlling bacterial infections by repelling or preventing their fouling,

* Corresponding author at: Physics Centre of Minho and Porto Universities (CF-UM-UP), Universidade do Minho, 4710-057, Portugal.
E-mail addresses: margaridafernandes@fisica.uminho.pt, margaridafernandes@cmems.uminho.pt (M.M. Fernandes).

https://doi.org/10.1016/j.ijbiomac.2023.125049
Received 28 September 2022; Received in revised form 15 May 2023; Accepted 21 May 2023
Available online 30 May 2023

particularly required for clinical settings [7,8]. Standard antibacterial coatings and surfaces have been produced using known antimicrobial agents, such as silver compounds [9,10], zinc oxide [11], copper and copper alloys [9], or organic molecules with quaternary ammonium chemical groups [12]. However, the side effects due to the leaching of these materials, represent a strong concern given their ecotoxicity and cytotoxicity towards mammalian cells [12]. In this context, natural-based materials have been widely investigated as suitable materials able to effectively interact with bacteria and overcome toxicity complications. In fact, natural compounds are in high demand due to their ability to minimize undesirable interactions between the material and the physiological environment while being environmentally friendly [13]. Antimicrobial peptides, natural quorum-sensing inhibitors, essential oils, or enzymes are some of the bioinspired compounds used so far to develop antibacterial coatings [14].

The use of natural polymers in the scope of sustainability of society and economy and to reduce environmental impact is also being explored [15]. In this sense, cellulose, as the most abundant natural polymer in the biosphere, emerges as an unbeatable candidate to fabricate natural multifunctional materials. This biopolymer can be easily modified with different functional groups to produce cellulose-derived materials with tailored applicability in diverse areas of technological and industrial relevance [16]. These applications include energy storage [17], sensing [16], water purification [18], tissue engineering [19], controlled drug release [20,21], anti-biofouling [22], and antibacterial coatings [23], among others. Cellulose nanocrystals (CNCs) in particular are cellulose derivatives obtained from the cell wall of cellulosic fiber and are typically regarded as isotropic polar nanoparticles with amphiphilic behavior in suspension [24].

CNCs have been incorporated into polymeric matrices and have been shown to significantly improve the mechanical and thermal properties of the hosting polymeric matrix when compared to other water-soluble cellulose derivatives [25]. This morphology, as rod-like and stiff nano-sized particles, can also be easily dispersed into biopolymers due to their small size, ranging from 5 to 10 nm in diameter and up to 300 nm in length [25,26].

Regarding the antibacterial properties of cellulose-based derivatives, amino-modified cellulose (aminocellulose) has shown promising properties. The underlying mechanism is similar to that of chitosan and is based on the electrostatic interactions between the positively protonated amino group (NH_3^+) of the biopolymer and negatively charged micro-organism membranes [27,28]. The positive-negative interaction results in intracellular component leakage and the consequent cell death. Aminocellulose possesses chitosan-like reactive groups on its surface able to disrupt the bacterial membrane [29–31] showing, interestingly, a higher antimicrobial activity than chitosan [28]. Moreover, chitosan has a problematic translation on an industrial scale due to the significant amount of alkaline waste produced during its manufacturing [27,32,33]. Thus, the amination of CNCs offers a rarely explored approach to obtaining antibacterial materials with improved physico-chemical properties, while preserving the inherent properties of cellulose.

Silk fibroin (SF) is another natural-based compound that has been increasingly used for biomedical applications. This protein displays several outstanding features that are useful not only for textile applications but also for the design and development of a wide range of biotechnological and biomedical devices [34,35]. Owing to its physicochemical properties, including excellent biocompatibility, biodegradability, minimal inflammatory reactions, and tunable mechanical properties, several works have focused on its potential for fabricating cell attachment supports, such as scaffolds [35,36]. SF-based scaffolds offer higher mechanical strength than other natural scaffolds, such as collagen, chitosan, and hyaluronan, making them a better candidate for tissue engineering, particularly for bone tissue engineering. This material has also been used as a surface coating on bone implants due to its high osteogenic activity in vitro and in vivo [37,38]. Furthermore, SF may be synergically combined with other materials to form SF-based materials with tailored properties.

The development of a fully natural renewable membrane based on amino-modified CNCs blended with SF is suggested in this work for the first time in the literature, to engineer an antibacterial and non-cytotoxic material. The SF/CNC-NH_2 blends are proposed to overcome bacterial infections by disrupting bacterial cell membranes – an antibacterial strategy to avoid resistance development – while increasing the efficacy of medical devices due to the presence of proteinaceous SF. Thus, the bactericidal activity of SF/CNC-NH_2 materials against *Staphylococcus epidermidis* and *Escherichia coli*, as well as their biocompatibility to a mammalian cell line, were investigated. The materials described herein represent a relevant and needed advance of the state-of-the-art in the field of antibacterial materials with practical value for clinical applications. In fact, the use of biomaterials that are inherently antimicrobial without the need for anchoring chemical approaches such as antibiotics is a promising and sustainable way of preventing surface-associated infections.

2. Materials and methods

2.1. Materials

Bombyx mori silkworm cocoons were supplied by APPACDM from Castelo Branco (Portugal). Cellulose nanocrystals, CNC, at 8 wt% in an aqueous suspension were provided by Blue Goose Biorefineries Inc. under the name BGB Ultra™. Sodium carbonate (Na_2CO_3), formic acid (FA, CH_2O_2), calcium chloride ($CaCl_2$), isopropanol (anhydrous, 99.5 %), *N*,*N*-Dimethylacetamide (DMA) (anhydrous, 99.8 %), p-Toluenesulfonyl chloride (TosCl) (≥99 %), lithium chloride (LiCl) (anhydrous, 99 %), triethylamine (Et_3N) (≥99.5 %) and ninhydrin reagent were purchased from Sigma-Aldrich. Distilled water was prepared in our laboratory. All reagents and solvents were used as received.

2.2. Synthesis of the pristine and blend membranes

2.2.1. Synthesis of the amino-modified CNCs

The amination of CNC to obtain CNC-NH_2 was carried out by the tosylation of the CNC and the subsequent nucleophilic displacement of p-toluenesulfonate with ethylenediamine (Fig. 1). The process used to synthesize tosyl-cellulose was described by Rahn et al [39]. First, 500 mg of CNC from an aqueous solution at 8 wt% were transferred to 20 mL of *N*,*N*-dimethylacetamide (DMA), followed by the dissolution of 1 g of LiCl. Then, 1.06 g of p-toluenesulfonyl chloride (TosCl) in the presence of 1.55 mL of triethylamine (Et_3N) was added and allowed to react at 8 °C for 24 h. After the tosylation, chemo- and regioselective nucleophilic substitution reaction take place by the addition of 20 Equiv. of the ethylenediamine dropwise, where the temperature of the reaction mixture was increased to 100 °C and stirred for 3 h [40]. The product was isolated by precipitation in 200 mL of water. The precipitate was filtered off and washed four times with 150 mL of isopropanol, four times with 150 mL water and finally dispersed in water. This solution was dried at room temperature over polyethylene Petri dishes obtaining a solid CNC-NH_2 suitable to produce pristine and blend membranes.

2.2.2. Extraction of silk fibroin

The degumming method was used for the extraction of silk fibroin (SF) from *Bombyx mori* silkworm cocoons [41]. Cocoons were selected, cleaned, cut into 2 cm^2 pieces, and boiled in a 0.05 wt% Na_2CO_3 solution for 30 min in silk to water solution ratio (*w*/*v*) of 1:40. The fibers of SF were washed with distilled water and dried at room temperature 24 h. Then, the fibers were dissolved in a 0.17 M solution of $CaCl_2$-formic acid with a ratio of 12:1 *v*/*w* (formic acid:SF). The solution was centrifuged at 6000 rpm for 10 min, to eliminate impurities. The supernatant SF/$CaCl_2$-formic acid solution was then cast on a glass Petri dish and left to dry at room temperature for 24 h, allowing the formic acid to evaporate.

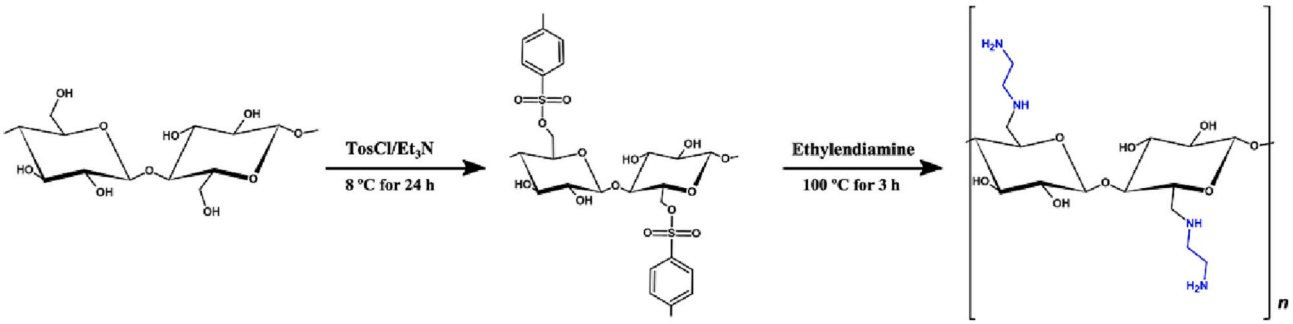

Fig. 1. Synthesis pathway of the amino-modified CNC-NH_2.

The resulting membrane was again washed in a distilled water bath to remove $CaCl_2$ and dried at room temperature, leading to a whitish solid SF. In the final step, SF was dissolved in neat formic acid (5:1 *v/w* formic acid:SF) to produce an SF/formic acid solution suitable for the preparation of pristine SF (Fig. 2) and blends.

2.2.3. Processing of the pristine and blend membranes

Pristine one-constituent membranes composed of SF or CNC-NH_2, with a thickness of 20–40 μm, were obtained by casting the solutions over two different polyethylene Petri dishes and dried at room temperature.

Blend membranes composed of SF and CNC-NH_2 were prepared to contain 5, 10, and 20 wt% of CNC-NH_2 and named SF/5CNC-NH_2, SF/10CNC-NH_2 and SF/20CNC-NH_2, respectively. These membranes were prepared by mixing the SF/formic acid solution, described above, with different ratios of CNC-NH_2. Once both polymers were completely dissolved under magnetic stirring, the solution was cast overnight in polyethylene Petri dishes and dried at room temperature to remove all the formic acid.

2.3. Physicochemical characterization of the membranes

The SF/CNC-NH_2 membranes were characterized in terms of morphology and physicochemical properties. For morphological characterization, the samples were analyzed on the surface (top view) and in cross-section using a HitachiS-4800 field-emission scanning electron microscope (FESEM) at an acceleration voltage of 5 kV. The cross-sections were obtained by immersing the membranes in liquid nitrogen for a few seconds and then cutting them transversally. Before imaging, samples were sputtered with a 10 nm-thin gold layer.

The surface wettability was assessed by contact angle measurements. The measurements were performed in a Neurtek OCA15EC Data Physics instrument with ultrapure water (3 μL droplets) as the test liquid. For each sample, at least three measurements were conducted in various sample locations, and the average contact angle was computed using the digital image.

Fourier transform infrared (FTIR) spectroscopy was performed at room temperature from 4000 to 600 cm^{-1} using a Spectrum Two spectrometer (PerkinElmer) linked with an attenuated total reflectance (ATR) (single reflection diamond, PerkinElmer) accessory. After 64 scans with a resolution of 4 cm^{-1}, spectra were recorded. The deconvolution of the spectral region corresponding to amide I was performed with OriginPro 8.1 software (OriginLab, Northampton), to assess the relative content of the secondary structures present in each sample. This region was fitted by linear baseline correction and 15 points with the Savitzky-Golay method were applied. The number of components and peak positions identified by the second derivative were used as starting parameters for curve fitting iteratively ($R^2 > 0.999$) with a Gaussian function using the Levenberg-Marquardt algorithm [42]. Curve fitting was performed with the same set of parameters across samples to achieve comparable secondary structure assignment. The contribution of each fitted component to the amide I band was calculated from the relative area of the hidden bands by integrating the area under the curve and normalizing for the total area of amide I.

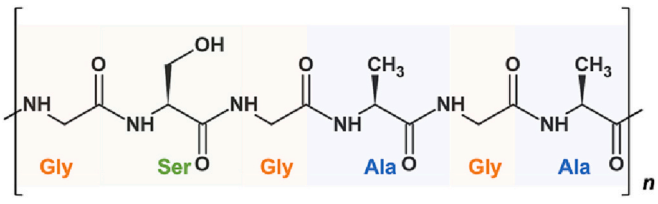

Fig. 2. Chemical structure of SF, depicting the amino acids serine (Ser), alanine (Ala), and glycine (Gly).

The presence of amino groups on the surface of the developed materials was visually determined using the ninhydrin reaction test. For this, sample pieces were placed in a tube containing 2 mL of a 2 % *w/v* ninhydrin solution and immersed in a 100 °C water bath for 5 min.

X-ray photoelectron spectroscopy (XPS) spectra were acquired using a system Versaprobe III Physical Electronics (ULVAC) equipped with a monochromated Al Kα X-ray source (1486.6 eV). An initial analysis was carried out to determine the elements present (wide scan: step energy 0.2 eV, pass energy 224 eV) and a detailed analysis of the detected elements was carried out (detail scan: step energy 0.05 eV, pass energy 27 eV, time per step 20 ms). The spectrometer was previously calibrated with Ag (Ag 3d5/2, 368.26 eV). Peak fitting of the measured spectra was performed by the CasaXPS software using Shirley background and Gaussian/Lorentzian line shapes (GL(30), 70 % Gaussian/30 % Lorentzian) without fixing peak parameters (binding energies (BE), full width at half maximum (FWHM) and area/intensity). Binding energies (BE) of photoelectron lines were determined with an accuracy of ±0.1 eV. Concentrations were calculated by correcting the values with relative atomic sensitivity factors (Scofield).

2.4. Antibacterial activity and cytotoxicity assessments

2.4.1. Antibacterial activity assessment

A Gram-positive *Staphylococcus epidermidis* (ATCC® 14990™) and a Gram-negative *Escherichia coli* (ATCC® 8739™), both acquired from American Type Culture Collection (LGC Standards S.L.U.), were used in the antibacterial experiments. A single colony from the corresponding stock bacterial culture was used to produce the bacterial pre-inoculum, which was then resuspended in nutrient broth (NB) and incubated overnight at 37 °C and 110 rpm. The optical density (OD) of *E. coli* and *S. epidermidis* cultures was evaluated at 600 nm after 16 to 20 h and adjusted in both cases, yielding a working inoculum of about 1×10^6 colony-forming units (CFU) per mL.

2.4.2. Antibacterial activity of the amino-modified CNCs at suspension

The antibacterial activity of the developed CNC-NH_2 at suspension was evaluated using the microdilution antimicrobial technique. Briefly,

different concentrations of CNC-NH_2 were generated by serial dilutions of a 50 % (*v*/v) CNC-NH_2 stock solution in sterile NB, using a 96-well microtiter plate. Then, each well was filled with an equal volume of bacterial inoculum, corresponding to approximately 1×10^6 CFU.mL^{-1}. Two different controls were performed: one with simply the bacterial inoculum and NB medium (control), and the other with only CNC-NH_2 and NB medium and no bacterial inoculum. The plates were further incubated at 37 °C for 24 h. Bacterial growth was measured using a microplate reader at 600 nm immediately after the microdilution procedure (T0h) and after 24 h of incubation (T24h). Cell viability was assessed using Eq. 1:

$$\text{Bacterial cell viability } (\%) = \frac{Abs_{sample\ T24h} - Abs_{sample\ T0h}}{Abs_{control\ T24h} - Abs_{control\ T0h}} \times 100 \quad (1)$$

2.4.3. Antibacterial activity of the developed membranes

The bacteriostatic activity of the developed materials was assessed according to the standard shake flask method (ASTM-E2149–01). After approximately 20 h, the bacterial suspension of the pre-inoculum was harvested twice by centrifugation at 5000 rpm for 5 min and resuspended in a buffer solution of NaCl 0.9 % (*w*/*v*). At 600 nm, the OD of bacterial cultures was measured and corrected to 0.36 ± 0.01 for *E. coli* and 0.28 ± 0.01 for *S. epidermidis*, yielding a working inoculum of 1×10^7 CFU.mL^{-1}. 1 cm × 1 cm segments of the samples were cut and sterilized with UV light before being placed in contact with 2 mL of bacterial suspension at 37 °C and 200 rpm for 2 h. Then, to determine the number of surviving bacteria, the suspensions were serially diluted in sterile buffer solution, plated on plate count NB agar, and incubated at 37 °C for 24 h.

This approach offers quantitative data for calculating the rate of decrease in the number of colonies formed, which is converted to the average colony forming units per milliliter of buffer solution in the flask (CFU.mL^{-1}). The results are expressed in percent log reduction, which is calculated as the ratio between the number of surviving bacteria with and without contact with the samples, according to Eq. 2.

$$Log\ reduction = log_{10}(A) - log_{10}(B) \quad (2)$$

where A and B are the average numbers of viable bacteria before and after contact with the samples, respectively. All antibacterial data represent mean values ± SD ($n = 3$).

2.4.4. Cytotoxicity assessment

The fibroblast L929 cell line was used for the cytotoxicity study, as indicated by the ISO10993-5 standard test procedure. In a 75 cm^2 cell culture flask, L929 fibroblasts were cultured in culture media (Dulbecco's Modified Eagle's Medium (DMEM, Gibco)) containing 4.5 g.L^{-1} glucose and supplemented with 10 % Fetal Bovine Serum (FBS, Biochrom) and 1 % Penicillin/Streptomycin (P/S, Biochrom). The culture flask was incubated at 37 °C and 5 % CO_2 in a humidified atmosphere. The culture medium was changed every two days till the confluence reached 60–70 %. The cells were then collected using trypsin-EDTA (Biochrom). The indirect cytotoxicity of the different processed materials was next examined. Similarly to the bacteriostatic activity evaluation, samples with 1 cm × 1 cm were cut and sterilized with UV light before being washed twice with a Phosphate-Buffered Saline (PBS) solution. Then, an extraction media was prepared by immersing the individual samples in a 24-well tissue culture polystyrene plate with culture media and incubating them for 24 h at 37 °C in humified air containing 5 % CO_2. Likewise, L929 fibroblasts were seeded at a density of 3×10^4 cells.mL^{-1} in a 96-well tissue culture and cultured under the conditions indicated above. After 24 h, the culture medium was withdrawn from the 96-well tissue culture polystyrene plate and the as-produced extraction medium was applied to the wells. Cell viability was evaluated using the 3-(4,5-dimethylthiazol-2-yl)-2,5-diphenyltetrazolium bromide (MTT) assay after 72 h of incubation. Thus, the media in each well was removed and 100 μL of 10 % MTT solution in DMEM (stock solution of 5 mg.mL^{-1} MTT in PBS) was added. After 2 h of incubation, viable cells convert MTT into a purple-colored formazan product, which may be quantified by dissolving the produced MTT crystals within the cells in dimethyl sulfoxide (DMSO, Sigma Aldrich). The OD at 570 nm was measured using a spectrophotometric plate reader (Biotech Synergy HT). All quantitative results from five replicate samples and controls were obtained and analyzed using Eq. 3:

$$\text{Cell viability } (\%) = \frac{Abs_{570nm}\ sample}{Abs_{570nm}\ negative\ control} \times 100 \quad (3)$$

3. Results and discussion

3.1. Morphological and physicochemical characterization

The surface topography and morphology of the samples were assessed using SEM. The representative micrographs of Fig. 3 demonstrate a dense and pore-free morphology with a similarly smooth, uniform, and neat surface for all the studied samples. The cross-section micrographs of the blends (inset Fig. 3c, d, and e), demonstrate a complete mixing between SF and CNC-NH_2 with no island-sea structure characteristic of a phase separation where a minor phase remains dispersed in a major continuous phase [43]. Overall, the inclusion of CNC-NH_2 does not influence the overall structure in terms of topography and morphology. Controlling colonization with antiadhesive surfaces which prevent bacteria fouling is an added benefit in the engineering and design of antimicrobial surfaces. Since the topography of the membranes is similar among all obtained samples, one can infer that it will not influence the bactericidal activity of the material. On the contrary, other factors will govern any possible antiadhesion or antimicrobial properties. In fact, bacterial adhesion and biofilm formation at a surface is a complex process regulated by several factors including roughness [44] and porosity [45]: smooth surfaces, such as those, are preferred to reduce the nonspecific protein binding and thus provide antiadhesion properties [46,47].

The contact angle was then measured to evaluate the surface wettability of the samples and the results are presented in Fig. 3f. Surface wettability is critically related to the antiadhesion properties of surfaces, in a similar way to topography. Superhydrophobic surfaces are usually associated with non-fouling properties while hydrophilic is commonly associated with facilitated protein and/or bacterial adhesion [48]. It is widely accepted that hydrophilic surfaces have contact angles with water $<90°$ while hydrophobic surfaces show angles $>90°$. As originating from CNCs, the CNC-NH_2 is a cellulose derivative with a high water affinity that can be readily dispersed in water [49]. In fact, the membranes solely consisting of CNC-NH_2 display absolute wetting properties and consequently, no contact angle could be measured. On the other hand, the contact angle of pristine SF membranes shows the opposite behavior, being near 90° (89 ± 5). The blends containing 5, 10, and 20 wt% CNC-NH_2 present contact angles of 85° ± 4, 74° ± 2, and 71° ± 2, respectively. As the CNC-NH_2 content increases, the water contact angle of the blends decreases, proving that the hydrophilicity of the membranes can be properly tailored.

Besides the primary structure of SF, the secondary structure also determines many of its material properties. The hydrophobic domains of SF chains are formed by repeating amino acid sequences (Gly-Ala-Gly-Ala-Gly-Ser) that are organized into nanocrystals (β-sheet). The amorphous part of the secondary structure is formed by the hydrophilic linkages between these hydrophobic domains, which are made up of bulky and polar side chains [50]. These characteristics are indicative that the introduction of CNC-NH_2 may interfere with the crystalline arrangement of the blends. Thus, the molecular structure of the produced membranes was evaluated using FTIR, and the obtained results are plotted in Fig. 4.

Fig. 4a shows that the main absorption bands of the samples remain constant across the whole range of FTIR measurements. Amide A ~

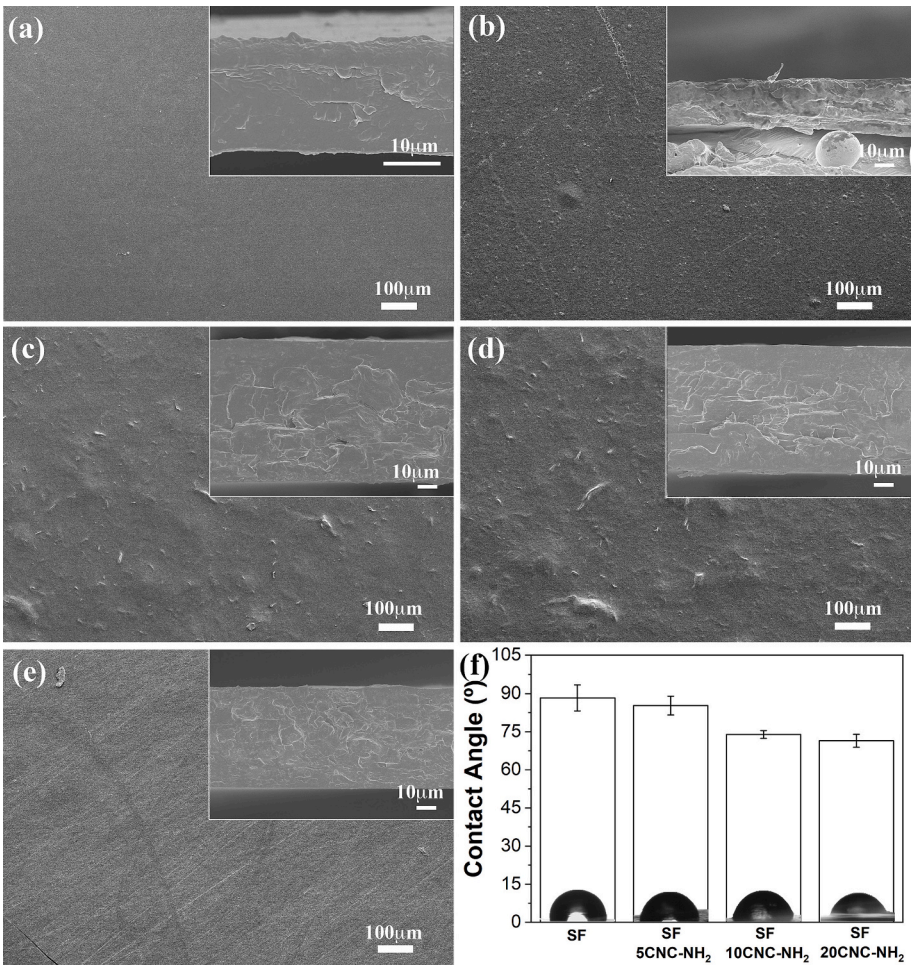

Fig. 3. Representative SEM images of the surface of pristine (a) SF and (b) CNC-NH_2 and blends (c) SF/5CNC-NH_2, (d) SF/10CNC-NH_2 and (e) SF/20CNC-NH_2, as well as (f) the respective measurements of the contact angles with water. The corresponding cross-section images are presented as insets.

3300 cm^{-1}, Amide *I* ~ 1620 cm^{-1}, Amide II ~ 1517 cm^{-1}, and Amide III ~ 1235 cm^{-1} are highlighted (Fig. 4a), as they are the most prominent absorption bands in the FTIR spectra of SF compounds [41,51,52].

Observing the CNC-NH_2 spectrum, the ranges corresponding to amides do not present relevant peaks, as expected. There are two absorption bands at 2900 and 1320 cm^{-1} caused by the C═O stretching and O—H bending vibrations typical of cellulose [29]. At 3334 and 3278 cm^{-1} (indicated with arrows), the CNC-NH_2 sample exhibits absorption bands corresponding to the cellulose O—H stretch and the secondary NH_2 amine group stretch, respectively [41,53]. The amine group vibrational mode at 3278 cm^{-1} is shared by all samples, while the hydroxyl peak at 3334 cm^{-1} is much less expressive in the remaining spectra (SF and blends). This absence in the blends may indicate the interaction of -OH from CNC-NH_2 with amino groups of SF, for the stabilization of the membrane material, which leaves the NH_3^+ available on the blends (Fig. 5c). This conclusion is supported by the analysis of the membranes with ninhydrin reagent, which reacts with primary and secondary amines at the surface of the materials. The formation of a deep blue color, frequently termed Ruhemann's purple, reveals the presence of amino groups [54]. There is a clear presence of amino groups at the surface of the material with increasing concentrations of CNC-NH_2 in the blend (Fig. 4c). It is noticed that the CNC-NH_2 alone does not show a blue color. Altogether these results suggest that when only CNC-NH_2 is present, the amino groups are used to stabilize the material thus being capped and not available at their surface (Fig. 5b). With the introduction of the SF, the stabilization is achieved with the amino groups from the amide groups of SF, thus leading the NH_3^+ groups from CNC-NH_2 available (Fig. 5c).

Regarding the other spectra, the relevant bands are amide A, I, II, and III, showing that the primary structure of SF is conserved (Fig. 5a). The secondary structure of SF was studied through an analysis of the amide I region at 1700–1580 cm^{-1} (Fig. 4b). This region corresponds to the most prominent and sensitive vibrational bands of the protein backbone, being related to C═O stretching vibration, CCN deformation, out of phase CN stretching vibration, and NH in plane bending [55]. A typical amide I deconvolution was applied to determine the relative amount of secondary structures, by fitting (hidden) peaks from the original spectra (Fig. 4d, as an example). The disclosed structures are β-sheets (1703–1697 and 1628–1615 cm^{-1}), random coils (1655–1628 cm^{-1}), α-helices (1662–1656 cm^{-1}), and turns (1696–1663 cm^{-1}) [55,56]. Hidden bands corresponding to the four structures appear in all data after peak fitting (Fig. 4e). β-sheet conformation is the most abundant, comprising >60 % of the total amide I peak area in all materials. Thus, according to the degree of crystallinity formula [57] for SF compounds, all membranes present crystallinity values exceeding 60 %. Fig. 4e also shows that as the CNC-NH_2 concentration in the blends increases, the preferred configuration corresponds to the β-sheet and turns motifs. On the other hand, the profile of α-helices and random coils – amorphous domains – exhibits the opposite behavior. The random coil conformation presents the highest drop, from 14 % to almost 0 %. Those findings corroborate that strong interactions (such as hydrogen bonds) between SF and CNC-NH_2 during the blending process trigger the conformational transition from amorphous to crystalline domains, due to the insertion of facial amphiphilic clusters of CNC-NH_2 on silk fibroin β-sheets, resulting

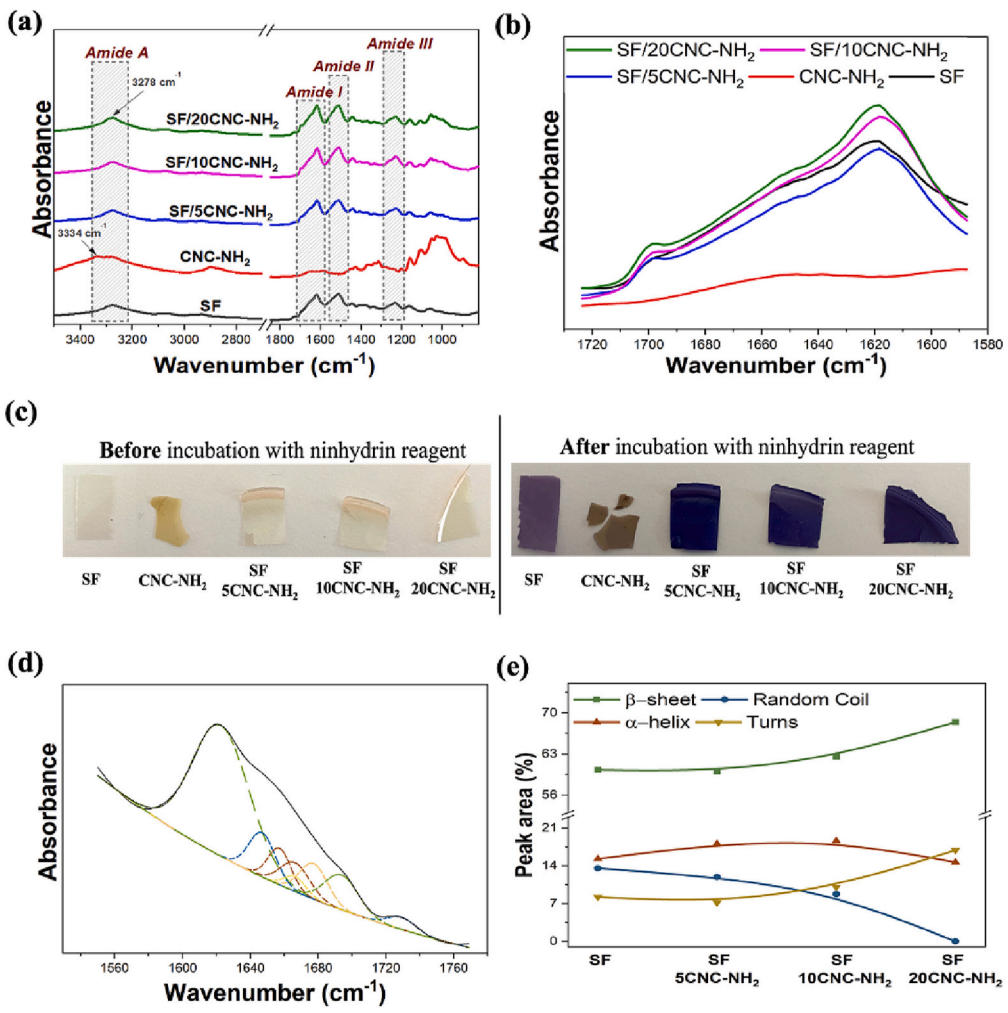

Fig. 4. (a) Full range FTIR spectra and (b) range corresponding to the amide I region for the different samples. (c) Photographs of pristine and blended sample pieces, before and after incubation with ninhydrin solution. (d) Representative amide I deconvolution spectrum for neat SF and (e) area fraction of the distinct components resolved in this spectral region. β-sheet (green), random coils (blue), α-helix (red), and turns (yellow) are the various contributions to the amide I structure. (For interpretation of the references to color in this figure legend, the reader is referred to the web version of this article.)

in the proposed chemical structure depicted in Fig. 5c [58,59]. The design of antimicrobial agents, e.g. antimicrobial peptides, based on clustering local facial amphiphilicity from repeating units, as herein reported, to obtain an enhanced interaction with bacterial membranes has been recently reported [60].

The chemical composition of the samples was confirmed by XPS measurements. Fig. 6a shows the wide scan XPS spectra which demonstrate the presence of C, O, and N elements. The C_{1s}, O_{1s}, and N_{1s} spectra were resolved into the different chemical bounds and the results can be analyzed in Table 1. The analysis of the carbonic region reveals three components in all samples, with this region having the highest atomic concentration, as predictable. Concerning the specific regions O_{1s} and N_{1s}, it becomes clear that these atomic concentrations increase as the CNC-NH_2 concentration increases in blends (Table 1). This fact highlights that blends present more O and N chemical bonds on the surface as previously observed by FTIR measurements in Fig. 4a. Moreover, the deconvolution of N_{1s} (Fig. 6b) XPS core level peaks recorded on the different samples displayed different characteristics. Comparing pristine samples with blends (Fig. 6b), it is possible to observe that only blends show an NH_3^+ peak (indicated with an arrow). According to the literature, peaks centered between 398 and 400 eV and 401 and 402 eV correspond to amine bonds and protonated cationic amine, respectively [61,62]. Knowing this, CNC-NH_2 acts as a deprotonating agent on the surface of SF, which also supports the FTIR analysis hypothesis: the interaction of -OH from CNC-NH_2 with amino groups of SF tends to leave the NH_3^+ available on the blends.

3.2. Antibacterial activity and cytotoxicity assessments

The antibacterial activity of a material is mainly determined by its intrinsic physicochemical properties. Amine cellulose derivatives have been reported as an antibacterial agent due to their positive charges that interact with negatively charged bacterial membranes inducing the disruption of the bacterial membrane [31,63]. Thus, to determine the extent of such action, the bactericidal effect of stand-alone CNC-NH_2 was initially evaluated (Fig. 7a).

The graph presented in Fig. 7a shows that the CNC-NH_2 suspension solution is characterized by a significant bactericidal effect in both Gram-positive and Gram-negative bacteria. *S. epidermidis* requires about 1 $mg.mL^{-1}$ to suppress cell growth by half when compared to the control, whereas *E. coli* demands twice the concentration to inhibit growth by only 30 %. This behavior is consistent throughout the tested concentrations, as *E. coli* always outperforms *S. epidermidis* in terms of cellular growth. In suspension, CNC-NH_2 appears to be more toxic against *S. epidermidis* than to *E. coli*, which could be correlated with the structural arrangement of their cellular membrane. Gram-positive *S. epidermidis* has a tick cell wall with an exposed peptidoglycan layer, while Gram-negative *E. coli* is characterized by a relatively thin cell covered by another protective outer membrane. These variations in the cell membrane impart distinct features to the cell, most notably in response to the external environment [64].

After proving the antibacterial effectiveness of the developed CNC-NH_2 in solution, the capability of the produced membranes to inactivate or kill bacteria by direct contact was also tested using the conventional

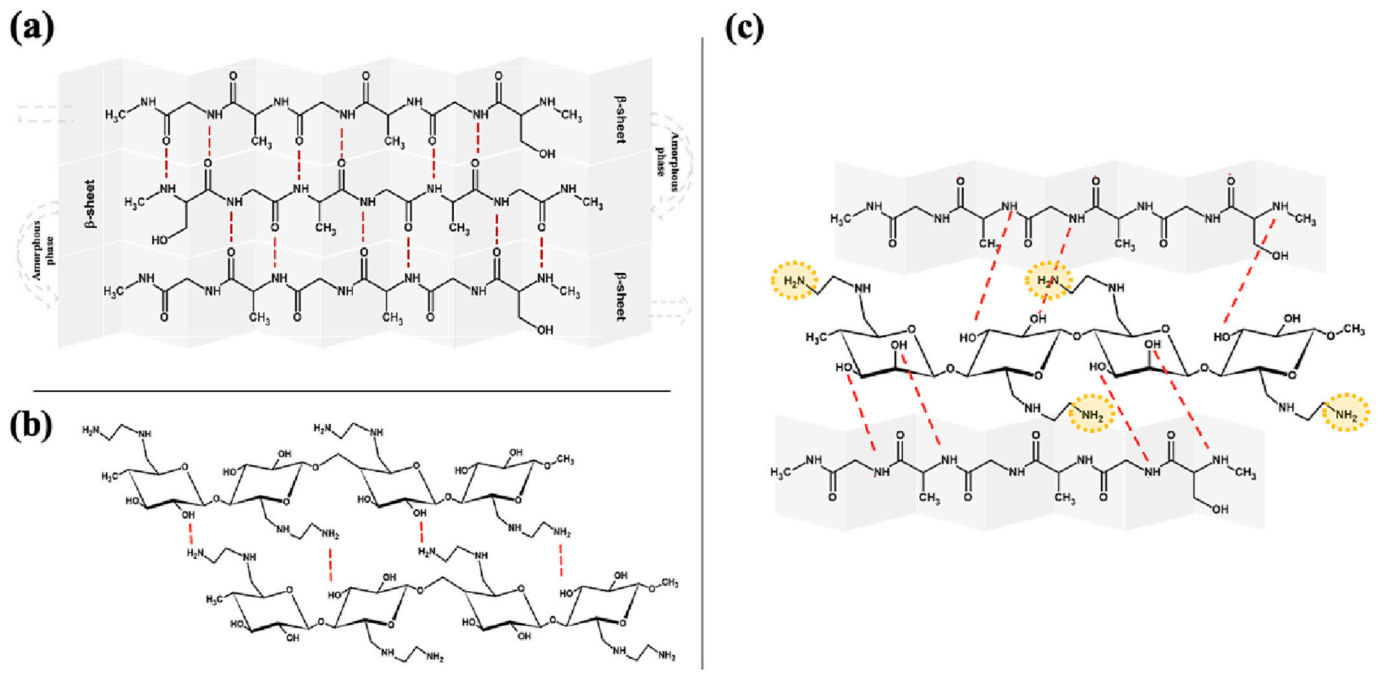

Fig. 5. Chemical structures of (a) pristine SF membranes in antiparallel β-sheet crystallites arrangement, (b) pristine CNC-NH_2 membranes, and (c) blends of SF/CNC-NH_2 showing the clusters of amphiphilic CNC-NH_2 with exposed amino groups in yellow. Hydrogen bonds are represented with a dashed red line. (For interpretation of the references to color in this figure legend, the reader is referred to the web version of this article.)

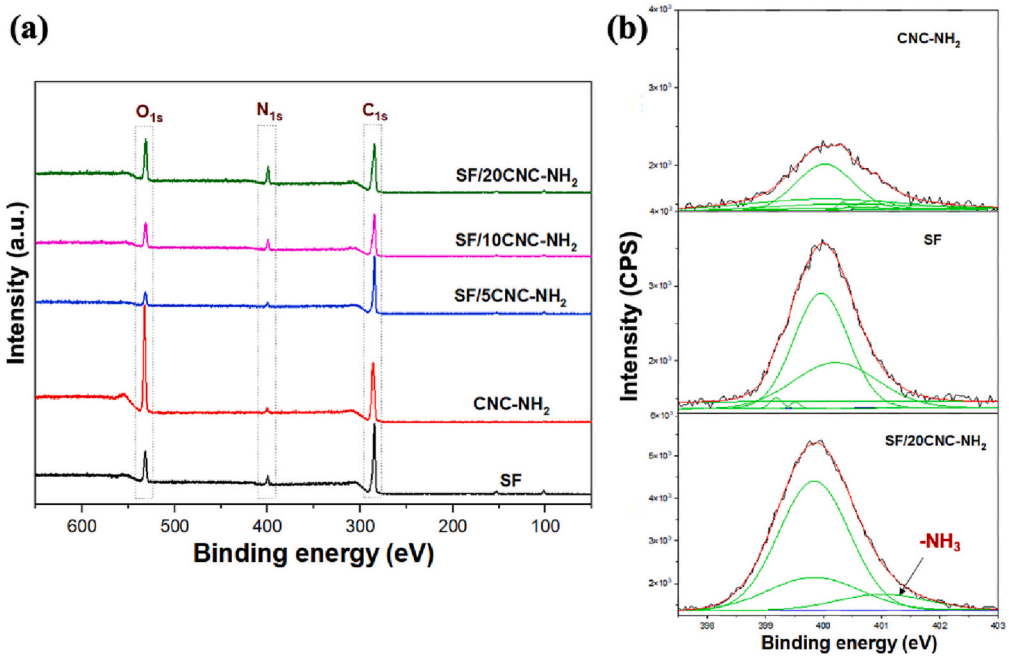

Fig. 6. XPS survey of (a) all samples with C_{1s}, $O_{1s,}$ and N_{1s} peaks highlighted and (b) deconvolution of N_{1s} for CNC-NH_2, SF, and SF/20CNC-NH_2 samples, as an example. The intensity is plotted in the y-axis as (a) arbitrary units (a.u.) and (b) counts per second (CPS).

shake flask method (AST E2149–01). According to the results shown in Fig. 7b, the relative number of inactivated bacteria, expressed using CFUs $\log_{10}$ reduction, are inexpressive when bacteria are in contact with membranes containing only one component: SF or CNC-NH_2. Both Gram bacteria present the same behavior in the presence of these materials. On the other hand, all the blends show the exact opposite response, exhibiting a strong antimicrobial effect and statistically significant when compared to pristine SF and CNC-NH_2. The SF/5CNC-NH_2 blend induces approximately a 2 $\log_{10}$ reduction on both bacteria, while blends with 10 and 20 wt% CNC-NH_2, the $\log_{10}$ reduction is approximately 2.5 and 3.5, respectively. These findings imply that as CNC-NH_2 concentration increases, so does the ability of the blends to kill both bacteria. According to the literature, amino groups are responsible for antimicrobial activity, thus the higher the number of these groups, the strong the antimicrobial activity [65]. In the case of membranes prepared solely of CNC-NH_2, they do not influence bacterial growth, corroborating the findings from FTIR and ninhydrin test, which indicate that the amino groups may be capped as depicted in Fig. 5b, rather than on the surface

Table 1
Binding energy (BE) and atomic concentration (AC) for fitted components of the samples.

		Chemical bonds						
		C-C/C-H	C-O/C-N	O-C=O/N-C=O	C=O	C-OH/O-H	C-NH-C/NH_2	NH_3^+
SF	BE	284.61	285.91	287.94	531.72	533.16	399.68	–
	AC %	56.29	13.13	8.79	11.63	2.65	7.52	–
		78.21			14.28		7.52	
CNC-NH2	BE	284.6	286.19	287.72	–	532.5	399.86	–
	AC %	20.35	33.65	10.66	–	32.92	2.42	–
		64.66			32.92		2.42	
SF5	BE	284.61	285.9	287.9	531.67	533.08	399.75	–
CNC-NH2	AC %	68.99	9.92	6.26	7.57	1.99	5.28	–
		85.17			9.56		5.28	
SF10	BE	284.6	285.95	287.95	531.57	532.95	399.81	401.01
CNC-NH2	AC %	45.84	17.57	10.95	12.13	3.49	8.59	1.43
		74.36			15.62		10.02	
SF20	BE	284.62	285.98	287.98	531.63	533.05	399.89	401.11
CNC-NH2	AC %	31.69	22.31	14.23	14.47	5.20	10.62	1.49
		68.23			19.67		12.11	

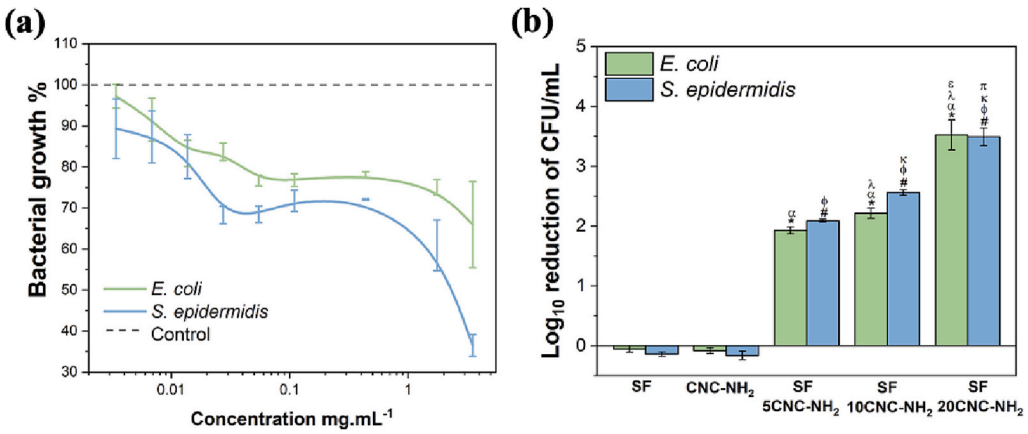

Fig. 7. (a) Dose-dependent effect of CNC-NH_2 in bacteria suspension culture and (b) bacterial cell reduction of both bacteria with respect to the control of freely growing bacteria. All results are the average of three or four independent assays. $^{*}P < 0.001$ and $^{\alpha}P < 0.001$ vs "SF" and "CNC-NH_2", respectively, against *E. coli*; $^{\#}P < 0.001$ and $^{\Phi}P < 0.001$ vs "SF" and "CNC-NH_2", respectively, against *S. epidermidis*; $^{\lambda}P < 0.001$ and $^{\varepsilon}P < 0.001$ vs "SF/5CNC-NH_2", and "SF/10CNC-NH_2", respectively, against *E. coli*; $^{\kappa}P < 0.001$ and $^{\pi}P < 0.001$ vs "SF/5CNC-NH_2", and "SF/10CNC-NH_2", respectively, against *S. epidermidis*.

of the membrane, available for interaction with bacteria as depicted in Fig. 5c [26].

The absence of cytotoxicity is a critical factor to consider when developing materials for biomedical purposes. Thus, the produced membranes were placed in contact with the cell culture media for 24 h, before being placed in contact with a cell culture of L929 fibroblasts for 72 h.

The data shown in Fig. 8 demonstrates that none of the samples are cytotoxic. All materials exhibit cell viability values above 70 %, which is the threshold according to ISO 10993-5. Membranes containing solely SF and CNC-NH_2 exhibit superior cell viability than the negative control, implying a possible ability to support cell proliferation [37]. Regarding blend membranes, cell viability remained nearly constant, even when the concentration of CNC-NH_2 in the blends was raised.

It is noteworthy that, despite the high antibacterial capacity of the blends, as evidenced by the 2 and 3 $\log_{10}$ reductions against the analyzed bacterial strains (Fig. 7b), these are completely biocompatible towards fibroblasts, which is a remarkable breakthrough.

4. Conclusion

Combating bacterial resistance is an urgent need, as well as promoting sustainability and decreasing the environmental impact of current materials and technologies. This investigation successfully proposes an entirely natural antibacterial and non-cytotoxic polymer blend with application in several fields and with good alignment with the circular economy. The putative advantages of the proteinaceous SF and CNC-NH_2 were herein considered and studied. In FTIR analysis, the CNC-NH_2 3334 cm^{-1} peak assigned to the hydroxyl group (-OH) vanishes in

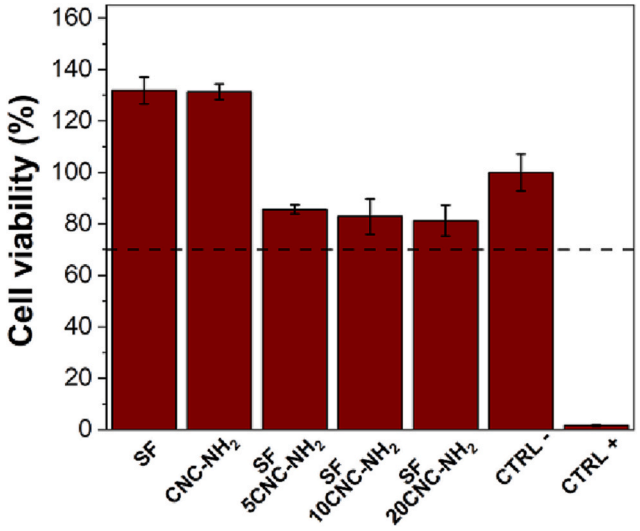

Fig. 8. Cytotoxicity assay results of the L929 fibroblast cells in contact with the media previously exposed to the developed membranes after 72 h. The dotted line denotes the 70 % threshold for cellular cytotoxicity. All results are the average of three or four independent assays.

blends, indicating the reaction of -OH from CNC-NH_2 with SF amino groups (from the amide functional group) and thus the availability of NH_3^+ groups in blends' surface. This assumption is also supported by

ninhydrin reagent analysis and XPS measurements. Moreover, the amino groups from the amide groups of SF are thought to ensure the stable conformation of the blends, thus inducing a higher crystallinity of the blend, when compared with SF membranes. Observing the antibacterial activity of the samples against *S. epidermidis* and *E. coli*, the bactericidal effect of the blends is confirmed. When both Gram bacteria are exposed to blends containing different ratios of CNC-NH_2, they experience different log reductions. The antibacterial activities increase as the surface amino groups also increase, with higher levels in blends containing 20 % wt. CNC-NH_2. Furthermore, this study disclosed that bacterial growth can only be inhibited by combining SF with CNC-NH_2. Ultimately, the synergy between these two environmentally friendly materials proves to be effective as an antibacterial without interfering with mammalian cell growth.

This work effectively addresses first-instance issues: decreasing global dependence on fossil fuel sources by replacing synthetic polymers and combating drug-resistant bacteria with alternative membrane disruption mechanisms. This blend may thus be transversally applied in different areas, from medical to food packaging or environmental applications, with no need for including external antimicrobial agents in the material. In a healthcare setting specifically, this strategy may pave the way for the prevention of nosocomial infections through the surface coating of indwelling medical devices or medically relevant surfaces. These types of antimicrobial materials, made of biopolymers that are intrinsically antibacterial, represent a promising and novel approach for reducing drug-resistant bacteria. The likelihood of such materials developing resistance is very low since they bind to the bacterial cell wall and form pores in the membrane, which is a completely different target for bacteria. Membranes with improved antimicrobial properties and biocompatible fit the current needs of industrial and academic research that focus on the circular economy and target the development of safe materials that are environmentally friendly and reusable, with long-lasting and antimicrobial properties. Overall, designing bio-based membranes that naturally expose antimicrobial amino groups through the clustering of amino-modified cellulose nanocrystals on silk fibroin β-sheets resulted in a highly antimicrobial material when compared to their individually assembled counterparts, which is valuable from the materials' point of view but also from the sustainability point of view.

Declaration of competing interest

Margarida M. Fernandes, Estela O. Carvalho, Ricardo Brito-Pereira reports financial support was provided by Fundação para a Ciência e Tecnologia. Mikel Rincon-Iglesias, Erlantz Lizundia, Senentxu Lanceros-Mendez reports financial support was provided by Spanish State Research Agency.

Acknowledgment

This work has been supported by FCT – Fundação para a Ciência e a Tecnologia (FCT) under the scope of the strategic funding of UID/FIS/04650/2020, project PTDC/BTM-MAT/28237/2017 and grants SFRH/BD/145455/2019 (EOC), SFRH/BD/140698/2018 (RBP) and SFRH/BPD/121464/2016 (MMF). The authors also acknowledge funding by Spanish State Research Agency (AEI) and the European Regional Development Fund (ERFD) through the project PID2019-106099RB-C43/AEI/10.13039/501100011033 and from the Basque Government Industry Department under the ELKARTEK program. Finally, the authors thank for the technical and human support provided by SGIker of UPV/EHU.

References

[1] R.C. Founou, L.L. Founou, S.Y. Essack, Clinical and economic impact of antibiotic resistance in developing countries: a systematic review and meta-analysis, PLoS One 12 (12) (2017).
[2] O.E. Petrova, K. Sauer, Escaping the biofilm in more than one way: desorption, detachment or dispersion, Curr. Opin. Microbiol. 30 (2016) 67–78.
[3] D.A. Rasko, V. Sperandio, Anti-virulence strategies to combat bacteria-mediated disease, Nat. Rev. Drug Discov. 9 (2) (2010) 117–128.
[4] N.A. Turner, B.K. Sharma-Kuinkel, S.A. Maskarinec, E.M. Eichenberger, P.P. Shah, M. Carugati, T.L. Holland, V.G. Fowler, Methicillin-resistant Staphylococcus aureus: an overview of basic and clinical research, Nat. Rev. Microbiol. 17 (4) (2019) 203–218.
[5] S. Bekri, F. Desriac, M. Barreau, T. Clamens, T. Gallavardin, P.L. Nahenec-Martel, J. Vieillard, Y. Datoussaid, N. Choukchou-Braham, O. Lesouhaitier, X. Franck, S. Leleu, New antibacterial cadiolide analogues active against antibiotic-resistant strains, Bioorganic and Medicinal Chemistry Letters 30 (21) (2020).
[6] A. Boulangé, J. Parraga, A. Galán, N. Cabedo, S. Leleu, M.J. Sanz, D. Cortes, X. Franck, Synthesis and antibacterial activities of cadiolides a, B and C and analogues, Bioorganic and Medicinal Chemistry 23 (13) (2015) 3618–3628.
[7] D. Campoccia, L. Montanaro, C.R. Arciola, A review of the biomaterials technologies for infection-resistant surfaces, Biomaterials 34 (34) (2013) 8533–8554.
[8] L. Wang, C. Hu, L. Shao, The antimicrobial activity of nanoparticles: present situation and prospects for the future, Int. J. Nanomedicine 12 (2017) 1227–1249.
[9] N. Ciacotich, R.U. Din, J.J. Sloth, P. Møller, L. Gram, An electroplated copper–silver alloy as antibacterial coating on stainless steel, Surf. Coat. Technol. 345 (2018) 96–104.
[10] C. Liao, Y. Li, S.C. Tjong, Bactericidal and cytotoxic properties of silver nanoparticles, Int. J. Mol. Sci. 20 (2) (2019).
[11] M. Fiedot-Toboła, M. Ciesielska, I. Maliszewska, O. Rac-Rumijowska, P. Suchorska-Woźniak, H. Teterycz, M. Bryjak, Deposition of zinc oxide on different polymer textiles and their antibacterial properties, Materials 11 (5) (2018).
[12] C.J. Ioannou, G.W. Hanlon, S.P. Denyer, Action of disinfectant quaternary ammonium compounds against Staphylococcus aureus, Antimicrob. Agents Chemother. 51 (1) (2007) 296–306.
[13] P. Muthukumaran, P. Suresh Babu, S. Karthikeyan, M. Kamaraj, J. Aravind, Tailored natural polymers: a useful eco-friendly sustainable tool for the mitigation of emerging pollutants: a review, Int. J. Environ. Sci. Technol. 18 (8) (2021) 2491–2510.
[14] K. Glinel, P. Thebault, V. Humblot, C.M. Pradier, T. Jouenne, Antibacterial surfaces developed from bio-inspired approaches, Acta Biomater. 8 (5) (2012) 1670–1684.
[15] C. Baillie, R. Jayasinghe, Green Composites: Waste and Nature-Based Materials for a Sustainable Future, Second edition, 2017.
[16] D.M. Correia, E. Lizundia, R. Meira, M. Rincón-Iglesias, S. Lanceros-Méndez, Cellulose nanocrystal and water-soluble cellulose derivative based electromechanical bending actuators, Materials 13 (2020) 2294.
[17] H. Glatz, E. Lizundia, F. Pacifico, D. Kundu, An organic cathode based dual-ion aqueous zinc battery enabled by a cellulose membrane, ACS Applied Energy Materials 2 (2) (2019) 1288–1294.
[18] M.A. Lucchini, E. Lizundia, S. Moser, M. Niederberger, G. Nyström, Titania-cellulose hybrid monolith for in-flow purification of water under solar illumination, ACS Appl. Mater. Interfaces 10 (35) (2018) 29599–29607.
[19] R. Tarrahi, A. Khataee, A. Karimi, Y. Yoon, The latest achievements in plant cellulose-based biomaterials for tissue engineering focusing on skin repair, Chemosphere 288 (2022).
[20] A. Mianehro, Electrospun bioscaffold based on cellulose acetate and dendrimer-modified cellulose nanocrystals for controlled drug release, Carbohydrate Polymer Technologies and Applications 3 (2022), 100187.
[21] F. Mohammadi, M. Montazer, A. Mianehro, N. Eslahi, M. Mahmoudi Rad, Preparation of antibacterial cellulose fabric via copper (II) oxide and corn silk (Stigma maydis) nanocomposite, Starch - Stärke (2022) 2200156, n/a(n/a).
[22] V.T. Noronha, J.C. Jackson, C.H.M. Camargos, A.J. Paula, C.A. Rezende, A.F. Faria, Attacking-attacking" anti-biofouling strategy enabled by cellulose nanocrystals-silver materials, ACS Applied Bio Materials 5 (3) (2021) 1025–1037.
[23] P. Tyagi, R. Mathew, C. Opperman, H. Jameel, R. Gonzalez, L. Lucia, M. Hubbe, L. Pal, High-strength antibacterial chitosan-cellulose nanocrystal composite tissue paper, Langmuir 35 (1) (2019) 104–112.
[24] S. Zuppolini, A. Salama, I. Cruz-Maya, V. Guarino, A. Borriello, Cellulose amphiphilic materials: chemistry, process and applications, Pharmaceutics 14 (2) (2022).
[25] M. Guo, S. Her, R. Keunen, S. Zhang, C. Allen, M.A. Winnik, Functionalization of cellulose nanocrystals with PEG-metal-chelating block copolymers via controlled conjugation in aqueous media, ACS Omega 1 (1) (2016) 93–107.
[26] J.A. Sirviö, M. Visanko, O. Laitinen, A. Ämmälä, H. Liimatainen, Amino-modified cellulose nanocrystals with adjustable hydrophobicity from combined regioselective oxidation and reductive amination, Carbohydr. Polym. 136 (2016) 581–587.
[27] A. Muñoz-Bonilla, C. Echeverria, Á. Sonseca, M.P. Arrieta, M. Fernández-García, Bio-based polymers with antimicrobial properties towards sustainable development, Materials 12 (4) (2019).
[28] M.M. Fernandes, A. Francesko, J. Torrent-Burgués, F.J. Carrión-Fité, T. Heinze, T. Tzanov, Sonochemically processed cationic nanocapsules: efficient antimicrobials with membrane disturbing capacity, Biomacromolecules 15 (4) (2014) 1365–1374.
[29] A. Francesko, K. Ivanova, J. Hoyo, S. Pérez-Rafael, P. Petkova, M.M. Fernandes, T. Heinze, E. Mendoza, T. Tzanov, Bottom-up layer-by-layer assembling of antibacterial freestanding Nanobiocomposite films, Biomacromolecules 19 (9) (2018) 3628–3636.

[30] K. Ivanova, A. Ivanova, E. Ramon, J. Hoyo, S. Sanchez-Gomez, T. Tzanov, Antibody-enabled antimicrobial Nanocapsules for selective elimination of Staphylococcus aureus, ACS Appl. Mater. Interfaces 12 (32) (2020) 35918–35927.
[31] A. Francesko, M.M. Fernandes, K. Ivanova, S. Amorim, R.L. Reis, I. Pashkuleva, E. Mendoza, A. Pfeifer, T. Heinze, T. Tzanov, Bacteria-responsive multilayer coatings comprising polycationic nanospheres for bacteria biofilm prevention on urinary catheters, Acta Biomater. 33 (2016) 203–212.
[32] M.Z. Elsabee, E.S. Abdou, Chitosan based edible films and coatings: a review, Mater. Sci. Eng. C 33 (4) (2013) 1819–1841.
[33] B. Bellich, I. D'Agostino, S. Semeraro, A. Gamini, A. Cesàro, "The good, the bad and the ugly" of chitosans, Marine Drugs 14 (5) (2016).
[34] P. Gupta, B.B. Mandal, Silk biomaterials for vascular tissue engineering applications, Acta Biomater. 134 (2021) 79–106.
[35] B. Kundu, R. Rajkhowa, S.C. Kundu, X. Wang, Silk fibroin biomaterials for tissue regenerations, Adv. Drug Deliv. Rev. 65 (4) (2013) 457–470.
[36] Y. Cetin, M.G. Sahin, F.N. Kok, Application potential of three-dimensional silk fibroin scaffold using mesenchymal stem cells for cardiac regeneration, J. Biomater. Appl. 36 (4) (2021) 740–753.
[37] H. Asadi, S. Ghalei, H. Handa, R.P. Ramasamy, Cellulose nanocrystal reinforced silk fibroin coating for enhanced corrosion protection and biocompatibility of mg-based alloys for orthopedic implant applications, Progress in Organic Coatings 161 (2021).
[38] F. Mottaghitalab, H. Hosseinkhani, M.A. Shokrgozar, C. Mao, M. Yang, M. Farokhi, Silk as a potential candidate for bone tissue engineering, J. Control. Release 215 (2015) 112–128.
[39] K. Rahn, M. Diamantoglou, D. Klemm, H. Berghmans, T. Heinze, Homogeneous synthesis of cellulose p-toluenesulfonates in N,N-dimethylacetamide/LiCl solvent system, Angew. Makromol. Chem. 238 (1996) 143–163.
[40] P. Berlin, D. Klemm, J. Tiller, R. Rieseler, A novel soluble aminocellulose derivative type: its transparent film-forming properties and its efficient coupling with enzyme proteins for biosensors, Macromol. Chem. Phys. 201 (15) (2000) 2070–2082.
[41] A. Reizabal, S. Gonçalves, R. Brito-Pereira, P. Costa, C.M. Costa, L. Pérez-Álvarez, J.L. Vilas-Vilela, S. Lanceros-Méndez, Optimized silk fibroin piezoresistive nanocomposites for pressure sensing applications based on natural polymers, Nanoscale Advances 1 (6) (2019) 2284–2292.
[42] H. Yang, S. Yang, J. Kong, A. Dong, S. Yu, Obtaining information about protein secondary structures in aqueous solution using Fourier transform IR spectroscopy, Nat. Protoc. 10 (3) (2015) 382–396.
[43] X.F. Wei, F. Nilsson, H. Yin, M.S. Hedenqvist, Microplastics originating from polymer blends: an emerging threat? Environ. Sci. Technol. 55 (8) (2021) 4190–4193.
[44] H. Tang, T. Cao, X. Liang, A. Wang, S.O. Salley, J. McAllister Ii, K.Y.S. Ng, Influence of silicone surface roughness and hydrophobicity on adhesion and colonization of Staphylococcus epidermidis, Journal of Biomedical Materials Research - Part A 88 (2) (2009) 454–463.
[45] J. Taxis, C. von Wilmowsky, B.J. Pedimonte, H.U. Beuscher, J. Ries, M. Kesting, T. Moest, The influence of nanoporous anodic aluminum oxide on the initial adhesion of Streptococcus mitis and mutans, Journal of Biomedical Materials Research - Part B Applied Biomaterials 108 (4) (2020) 1687–1696.
[46] D. Perera-Costa, J.M. Bruque, M.L. González-Martín, A.C. Gómez-García, V. Vadillo-Rodríguez, Studying the influence of surface topography on bacterial adhesion using spatially organized microtopographic surface patterns, Langmuir 30 (16) (2014) 4633–4641.
[47] A. Uneputty, A. Dávila-Lezama, D. Garibo, A. Oknianska, N. Bogdanchikova, J. F. Hernández-Sánchez, A. Susarrey-Arce, Strategies applied to modify structured and smooth surfaces: a step closer to reduce bacterial adhesion and biofilm formation, Colloids and Interface Science Communications 46 (2022).
[48] E.J. Falde, S.T. Yohe, Y.L. Colson, M.W. Grinstaff, Superhydrophobic materials for biomedical applications, Biomaterials 104 (2016) 87–103.
[49] E. Lizundia, D. Puglia, T.D. Nguyen, I. Armentano, Cellulose nanocrystal based multifunctional nanohybrids, Prog. Mater. Sci. 112 (2020).
[50] Y. Qi, H. Wang, K. Wei, Y. Yang, R.Y. Zheng, I.S. Kim, K.Q. Zhang, A review of structure construction of silk fibroin biomaterials from single structures to multi-level structures, Int. J. Mol. Sci. 18 (3) (2017).
[51] Y. Ji, X. Yang, Z. Ji, L. Zhu, N. Ma, D. Chen, X. Jia, J. Tang, Y. Cao, DFT-calculated IR spectrum amide I, II, and III band contributions of N-methylacetamide fine components, ACS Omega 5 (15) (2020) 8572–8578.
[52] I.C. Um, H. Kweon, Y.H. Park, S. Hudson, Structural characteristics and properties of the regenerated silk fibroin prepared from formic acid, Int. J. Biol. Macromol. 29 (2) (2001) 91–97.
[53] W. Qiu, W. Teng, J. Cappello, X. Wu, Wet-spinning of recombinant silk-elastin-like protein polymer fibers with high tensile strength and high deformability, Biomacromolecules 10 (3) (2009) 602–608.
[54] M. Friedman, Applications of the Ninhydrin reaction for analysis of amino acids, peptides, and proteins to agricultural and biomedical sciences, J. Agric. Food Chem. 52 (3) (2004) 385–406.
[55] O.S. Rabotyagova, P. Cebe, D.L. Kaplan, Role of polyalanine domains in β-sheet formation in spider silk block copolymers, Macromol. Biosci. 10 (1) (2010) 49–59.
[56] B.D. Lawrence, F. Omenetto, K. Chui, D.L. Kaplan, Processing methods to control silk fibroin film biomaterial features, J. Mater. Sci. 43 (21) (2008) 6967–6985.
[57] Z. Shao, F. Vollrath, J. Sirichaisit, R.J. Young, Analysis of spider silk in native and supercontracted states using Raman spectroscopy, Polymer 40 (10) (1999) 2493–2500.
[58] S. Shang, L. Zhu, J. Fan, Physical properties of silk fibroin/cellulose blend films regenerated from the hydrophilic ionic liquid, Carbohydr. Polym. 86 (2) (2011) 462–468.
[59] G. Yang, L. Zhang, Y. Liu, Structure and microporous formation of cellulose/silk fibroin blend membranesI. Effect of coagulants, J. Membr. Sci. 177 (1–2) (2000) 153–161.
[60] M.A. Rahman, M. Bam, E. Luat, M.S. Jui, M.S. Ganewatta, T. Shokfai, M. Nagarkatti, A.W. Decho, C. Tang, Macromolecular-clustered facial amphiphilic antimicrobials, Nat. Commun. 9 (1) (2018).
[61] A. Mianehro, Electrospun bioscaffold based on cellulose acetate and dendrimer-modified cellulose nanocrystals for controlled drug release, Carbohydrate Polymer Technologies and Applications 3 (2022).
[62] L.R. Arcot, M. Lundahl, O.J. Rojas, J. Laine, Asymmetric cellulose nanocrystals: thiolation of reducing end groups via NHS–EDC coupling, Cellulose 21 (6) (2014) 4209–4218.
[63] T. Genco, L.F. Zemljič, M. Bračič, K. Stana-Kleinschek, T. Heinze, Physicochemical properties and bioactivity of a novel class of cellulosics: 6-deoxy-6-amino cellulose sulfate, Macromol. Chem. Phys. 213 (5) (2012) 539–548.
[64] A. Mai-Prochnow, M. Clauson, J. Hong, A.B. Murphy, Gram positive and Gram negative bacteria differ in their sensitivity to cold plasma, Sci. Rep. 6 (2016).
[65] M. Másson, J. Holappa, M. Hjálmarsdóttir, O.V. Rúnarsson, T. Nevalainen, T. Järvinen, Antimicrobial activity of piperazine derivatives of chitosan, Carbohydr. Polym. 74 (3) (2008) 566–571.